Article:
Collier, G.J. and Wild, J.M. orcid.org/0000-0002-7246-8660 (2015) In vivo measurement of gas flow in human airways with hyperpolarized gas MRI and compressed sensing. Magnetic Resonance in Medicine, 73 (6). pp. 2255-2261. ISSN 0740-3194

https://doi.org/10.1002/mrm.25348

Observation of cardiogenic flow oscillations in healthy subjects with hyperpolarized ^{3}He MRI

Guilhem J. Collier, Helen Marshall, Madhwesha Rao, Neil J. Stewart, David Capener, Jim M. Wild*

Academic Unit of Radiology, University of Sheffield, Royal Hallamshire Hospital, Sheffield, UK

Running Head: Observation of cardiogenic flow oscillations with HP ^{3}He MRI

*Correspondence to: Jim M. Wild, Ph.D., Academic Radiology, "C" floor, Royal Hallamshire Hospital, University of Sheffield, Glossop Road, S10 2JF, Sheffield, UK. Telephone: +44 114 226 5389. E-mail: j.m.wild@sheffield.ac.uk

Abstract:

Recently, dynamic MR imaging of hyperpolarized ^{3}He during inhalation revealed an alternation of the image intensity between left and right lungs with a cardiac origin (Respiratory Physiology & Neurobiology: 185, 468-471,2013). This effect is investigated further using dynamic and phase contrast flow MR imaging with inhaled ^{3}He during slow inhalations (flow rate ~ 100 mL s^{-1}) to elucidate air-flow dynamics in the main lobes in six healthy subjects. The ventilation MR signal and gas inflow in the left lower part of the lungs was found to oscillate clearly at the cardiac frequency in all subjects, whereas the MR signals in the other parts of the lungs had a similar oscillatory behavior but were smaller in magnitude and in anti-phase to the signal in the left lower lung. The airflow in the main bronchi showed periodic oscillations at the frequency of the cardiac cycle. In four of the subjects, backflows were observed for a short period of time of the cardiac cycle, demonstrating a pendelluft effect at the carina bifurcation between the left and right lungs. Additional ^{1}H structural MR images of the lung volume and synchronized ECG recording revealed that maximum inspiratory flow rates in the left lower part of the lungs occurred during systole when the corresponding left lung volume increased whereas the opposite effect was observed during diastole with gas flow being redirected to the other parts of the lung. In conclusion, cardiogenic flow oscillations have a significant effect on regional gas flow and distribution within the lungs.

Keywords: Cardiogenic oscillations, MRI, hyperpolarized gases, flow, lungs

Introduction

In the literature, the term cardiogenic oscillation has been used to refer to the modulation of the pulmonary gas pressure, flow or concentration produced by the cardiac cycle. Cardiogenic

oscillations have been intensively observed and recorded in the past in the context of pulmonary physiology measurements made at the mouth with pressure transducers, pneumotachographs (1, 20, 29) or gas analyzers (6, 15) but also directly inside the intra-thoracic airways during bronchoscopy (30). The cardiac cycle is thought to be an important component of gas mixing within the lung (12, 13, 15) and leads to oscillations in the concentration of oxygen and carbon dioxide in expired gas (5, 6). The cardiac action has therefore an uncontested influence on lung function but it is unclear how the different observations of cardiogenic oscillations are related to each other. In the present study, only cardiogenic flow oscillations (CO_f) present in the conducting airways are considered. CO_f can be detected in most subjects during the whole breathing cycle and in all regions of the lung (11). However, very little data has been published on the influence of CO_f on airflow pattern and gas distribution within the lung.

On the other hand, the field of study of pulmonary airflow has recently benefited from advancements in imaging and computation methodology. Computational fluid dynamics (CFD) simulations using realistic image-based airway models have vastly improved general understanding of the local characteristics of gas flow in the airways (25). These findings are of particular interest for inhaled therapy research (4) or the study of regional deposition of particles (17) but have yet to take into account realistic physiological features such as CO_f and have traditionally relied only on validation with in vitro airway tree models (21). In vivo, rates of gas ventilation in the main airways and the periphery can be assessed with dynamic hyperpolarized (HP) ^{3}He ventilation imaging (16, 31). In addition, phase contrast velocimetry (PCV) sequences can be used to directly map flow velocity profiles in the major airways (3, 10, 19). Sun et al. (24) recently performed dynamic ^{3}He ventilation imaging on seven healthy subjects and revealed an alternation of the MR image intensity between the left and right lung (“ventilatory alternans”)

with a periodicity approximating the heart rate (unmeasured), which was presumably the effect of cardiogenic flow oscillations. The aim of the present study is to further explore this phenomenon by performing dynamic HP ^{3}He ventilation imaging during inspiration in healthy subjects to assess the extent to which cardiogenic flow oscillations can influence the gas distribution inside the lobes and, additionally, by measuring gas velocities inside the main bronchi with PCV sequences to investigate the airflow pattern within the lungs.

Materials and Methods

Subject Characteristics, ^{3}He Production and Administration

Six healthy volunteers were recruited for this study (demographics and pulmonary function test results shown in Table 1). Approval from the national research ethics committee was obtained for all experiments. ^{3}He (Linde Gases, Huntingdon, UK) was polarized on site with a regulatory approved spin exchange polarizer to ~ 25 % (GE Healthcare, Amersham, UK). A 1 L gas mixture of N_2 and HP ^{3}He was delivered for the subjects to inhale inside the MRI scanner. The subjects performed a slow and constant-rate inspiration (inhalation time varied from 8 s to 15 s between subjects) from a Tedlar bag (Jensen Inert Products, Coral Springs, FL) containing 20 % of HP ^{3}He for dynamic ventilation and 30 % for phase contrast velocimetry imaging. Data were acquired during inhalation.

Image Acquisition

Imaging experiments were performed on a GE HDx 1.5T MR scanner with a maximum gradient strength of 33 mT m^{-1} and slew rate of 120 mT m^{-1} ms^{-1}. A quadrature flexible transmit-receive (T-R) ^{3}He radiofrequency coil (CMRS, Brookfield, WI) was used for dynamic ventilation and

1D velocity profile measurements. For 2D flow imaging across the left main bronchus, a home-built dedicated loop-butterfly quadrature T-R coil with high quality factor ($Q_{loaded}/Q_{unloaded}$ ~ 230/25) was used (see Fig. 1). The heartbeat of the subjects was monitored during all experiments with a finger probe or an ECG. When ECG was available (see Table 1), the R-wave occurrences were recorded during the imaging sequences. Sequence details were as follows:

- Dynamic ventilation imaging: Dynamic coronal images of the 6 healthy subjects were obtained with a spoiled gradient echo sequence (40×32 cm^2 field of view, 64 readout × 52 phase encode matrix, Cartesian sequential phase encoding, single slice, 25 cm thickness, echo/repetition time T_E/T_R of 0.8/2.7 ms, ± 31.25 kHz bandwidth, 3° flip angle and 150 frames with a time resolution per frame of 140 ms).
- 1D velocity profile imaging: Axial 1D projections, across the anterior to posterior direction, below the carina (see slice location 1, dashed line in the inset of Fig. 1) were acquired in the 6 subjects with a PCV sequence, providing dynamic 1D velocity profiles across the left and right main bronchi. A field of speed (FOS) of [-120, +120] cm s^{-1} was chosen along the superior to inferior direction which is the principal direction of gas flow (20 cm field of view, 128 points, 1 cm slice thickness, 20° flip angle and 768 frames with a 20 ms time resolution).
- 2D flow imaging: A 2D oblique slice through the left main bronchus (see slice location 2, solid line in the inset of Fig. 1) was imaged in subjects 1, 5 and 6 with a PCV sequence. The field of speed was set to [-160, +160] cm s^{-1} in the direction of the axis of the left main bronchus (5×3.75 cm^2 FOV, 32×18 matrix with a partial Fourier factor of 0.75 in the phase direction and sequential Cartesian phase encoding, 1.5 cm slice thickness,

T_E/T_R of 3.3/6.4 ms, ± 15.63 kHz bandwidth, 18° flip angle and 232.4 ms time resolution per image frame).

- Cardiac gated proton lung imaging: In order to observe the deformation of the lungs around the heart during the cardiac cycle, a standard cine cardiac gated balanced steady state free precession ^{1}H pulse sequence was used to obtain an axial stack of images of the lungs in the 6 subjects during breath hold (30 cm field of view, 256×256 matrix, 1 cm slice thickness, 60° flip angle, T_E/T_R of 1.8/4.3 ms and 20 heart phases).

Image Analysis

For the dynamic ventilation images, four regions of interest (ROIs) in the Right/Left Upper/Lower parts of the Lungs (RUL/LUL/RLL/LLL, see inset of Fig. 2A) were chosen and the time evolution of the ^{3}He MR signal was computed in each. The mean signals in each ROI were divided by the noise estimated from the first image of the experiment (acquired before inhaling ^{3}He) to compute signal to noise ratio (SNR) values. A Fourier analysis was performed for each SNR-time curve to detect the frequency of signal oscillations. The phase difference between signals at the fundamental frequency was also computed (the phase of the LLL signal was taken as a reference). Cardiac gated proton images were analyzed with ScanIP (Simpleware, Exeter, UK) to segment the volume of the lung cavity for each of the twenty cardiac frames. Pulmonary veins and arteries were not excluded. The relative volume changes ($V(t)/V_{mean}$) of the left and right lungs around the heart during the cardiac cycle were derived from the segmentation.

For the PCV data, velocity maps and profiles were generated offline from the raw data using in-house software developed in Matlab (MathWorks, Natick, MA). The phase difference reconstruction was performed using the two interleaves of each frame to extract the ^{3}He gas

velocity component in the encoded direction for each pixel. ROIs corresponding to the left and right main bronchi were selected manually and the time evolution of the average gas velocity was calculated for each 1D profile. For the 2D flow imaging experiments, the flow was derived by integrating the velocities over the area of the left main bronchus. An error analysis of the 1D average gas velocity and 2D flow values was performed. The following formula gives the statistical uncertainty of the velocity value derived from the phase difference reconstruction:

$$\boldsymbol{\sigma_v = \frac{FOS}{2\pi}\sqrt{(\sigma/S_1)^2 + (\sigma/S_2)^2}} \quad \textbf{(1)}$$

where S_1 and S_2 are the magnitude values of the two interleaves and σ is the standard deviation of the noise (the same in both interleaves). In practice $S_1 \sim S_2$ and the uncertainty in each velocity value is therefore inversely proportional to the signal of each corresponding pixel. Since the signal intensity is velocity dependent, the standard deviation of the velocity between pixels can be fairly different. Indeed, the volume of gas in a pixel experiencing high flow rate is renewed with "fresh" polarized gas (that has not undergone radio frequency destruction) more rapidly, whereas pixels with low flow rate have lower signal and therefore higher variance σ_v^2. The variance of the 2D flow measurement was calculated from the sum of each pixel variance multiplied by the pixel area, whereas the variance of the 1D average velocity measurement was derived according to the following formula:

$$\boldsymbol{\sigma_{av}^2 = \left(\sum_{ij}^{n} \sigma_{vij}^2\right)/n} \quad \textbf{(2)}$$

where σ_{vij} is the standard deviation of the pixel ij and n is the number of pixels in the selected ROI.

Results

Dynamic Ventilation: The signal to noise ratio (SNR) and hence, gas inflow in the left lower part of the lung was clearly found to oscillate at the cardiac frequency in all subjects (see Fig. 2, Fig. 4, Table 2 and supplementary material for videos of dynamic ventilation images of each subject). The signals in the other parts of the lungs (RLL, RUL and LUL) were also found to oscillate at the same frequency in 5 of the 6 subjects, but with a markedly different phase when compared to the LLL signal (139° was the average phase difference for the LUL signal, 167° for RLL and 145° for RUL). For subject 5 (Fig. 2F), no obvious pulsation was observed in the time evolution of RLL, RUL and LUL SNRs. The simultaneous ECG recording in subjects 2, 3, 5 and 6 showed that the R-wave occurrences corresponded to a minimum of SNR in the LLL (maximum SNR in the other regions for subjects 2, 3 and 6) and were followed by a rapid rise of the LLL signal.

1D Velocity Profile: Although the experiments were performed during constant inhalation, the average velocities in the left and right main bronchi fluctuated dramatically with a periodic pattern whose frequency matched the heartbeat (see Fig. 3 and Fig. 4). The recorded velocities ranged from -50 to 150 cm s^{-1} and varied antagonistically. More surprisingly, negative values (backflows) were measured during a small part of the cardiac cycle in subjects 1, 3, 4 and 6, demonstrating a pendelluft effect at the carina bifurcation between the left and right lungs. Although the periodic patterns were quite different between subjects, recordings of R-waves (start of systole) always preceded a strong gas inflow period in the left lung (low inflow or backflow in the right lung) whereas the opposite phenomenon happened at the beginning of diastole. The mean uncertainty in the measured average velocity value was found to be ± 6 cm s^{-1}.

2D Flow: Measured velocity maps from the LMB confirmed the periodicity and dramatic change of gas flow pattern during the cardiac cycle (see Fig. 5) and the existence of backflow in subjects

1 and 6. Flow values ranged from -40 to 220 mL s^{-1}. For subject 6, the ECG was recorded simultaneously and the maximum flow rate into the left lung was observed after the R-wave occurrence. σ_v was ~ 5 cm s^{-1} and the uncertainty on the flow values was below ± 2 mL s^{-1}.

Proton Imaging: Manual segmentation of left and right lung cavities surrounding the heart exhibited a similar relative volume time evolution for all subjects (see Fig. 6 and online supplementary material for a video of the lung segmentation of subject 1 through the cardiac cycle). During systole, the segmented lung volume increased on average by about 53 mL, which agrees well with the volume displaced per heartbeat of 60 mL quoted by Cotes et al. (5). Interestingly, 83 % of this increase was found in the left lung. The volume contraction of the heart ventricles corresponded to a left lower lung expansion confirmed by the displacement of the pulmonary vasculature in the left lung around the heart (see online supplementary video). During the first half of diastole, the opposite effect occurred with a similar rate of volume change as during systole (see inset of Fig. 6). The second part of diastole did not show major lung volume changes.

Discussion

In this study, a dramatic effect of cardiogenic flow oscillations on pulmonary airflow pattern was observed in the lungs of normal subjects with functional ^{3}He MR imaging. Whereas Sun et al. (24) noticed a 'ventilatory alternans' between the left and right lungs during inspiration in healthy subjects, our data suggest that this observation is the consequence of stronger flow oscillation in the left lower part of the lung due to the proximity of the heart, with accompanying weaker oscillations of opposite phase in the rest of the lungs. We believe that Sun et al. did not observe this localized origin most probably because of their choice of region of interest in the left

lung. The figure 1A of that study clearly shows that the left upper part of the lung was omitted in the signal intensity calculation. However, the dynamic images from the subjects in that study (available as videos in the online supplementary material) showed an alternans between the upper and lower parts of the left lung. The increase in time resolution in the dynamic ventilation imaging protocol between Sun et al. and the present studies (from 2.5 to 7.1 frames per sec) also better facilitates the visualization of the alternans. Our data are also in agreement with previous reports suggesting that the phase of CO_f is different in different parts of the lungs and that they are more marked on the left side (30). Interestingly, the phase of the LUL signal seems to change slightly in one subject (see Fig. 2A), which suggests that the phase difference between the lower and upper parts of the left lung could depend on the lung inflation level in some cases. The signal oscillations could be observed in all subjects in the LUL but only in 5 of 6 subjects in the rest of the lungs. Similarly, the ventilatory alternans and the CO_f were observed in 5 of 7 subjects in the imaging study of Sun et al. (24) and in 75 % of patients in a study by West et al. (30) with a gas flow meter, which confirms that the existence and/or severity of CO_f are subject dependent. However, it is worth noting that certain experimental and physiological conditions such as low flow rates, hyperinflated lungs (13), higher cardiac output per beat and lower heartbeat frequencies are more favorable for the observation of cardiogenic oscillations. Subject 5 performed a more rapid inhalation and had a faster heartbeat rate than the other subjects, which could partly explain why no clear signal oscillations could be detected in the rest of that subject's lungs.

In addition to dynamic ventilation imaging, the PCV MRI technique was developed to observe the effect of cardiogenic oscillations on the gas flow in the left and right main bronchi, which revealed the existence of a pendelluft effect. The ^{3}He gas velocity and flow values in the left and

right main bronchi were found to oscillate antagonistically and reversed backflows were recorded in 4 of 6 subjects. The shape of the flow patterns, although having common features, were different for all subjects. Among all subjects, the average velocity in both left and right main bronchi during the cardiac cycle was about 38.7 cm s^{-1}. Assuming a Weibel cross section of the airway with an area of 1.17 cm^2 for each main bronchus, and neglecting the fact that the slice is not fully perpendicular to the bronchi directions (see slice location 1 in the inset of Fig. 1), an average flow of 91 mL s^{-1} can be derived. This is roughly consistent with the expected average flow of 85 mL s^{-1} deduced from the average time of 11.8 s that was required by the subjects to inhale the 1 L bag of gas. PCV measurements have some limitations and possible scope for improvements. It would be desirable to perform flow measurement at the entrance of the main lobes and not only through the main bronchi, however, the localization of smaller airways is highly challenging given the quality and resolution of MRI. In addition, in order to deduce the exact flow pattern produced by CO_f, the measurement should also be repeated during breath hold. However, because the ^{3}He signal is nonrenewable, fresh gas needs to flow constantly through the ROI, which led us to a dynamic experiment during the inspiratory phase. Nevertheless, estimates of maximum CO_f values in the left main bronchus can be obtained from the 2D PCV measurements by inspection of the amplitude of the flow oscillations: approximately 45 mL s^{-1} for subjects 1 and 5 and 70 mL s^{-1} for subject 6. These results are reasonably consistent with previously reported volume flow rates of 42 mL s^{-1} (30). The addition of simultaneous ECG recording with MR measurements showed that some features in the CO_f pattern were common to all subjects. Maximum flow rates in the left lower part of the lung occurred during systole whereas the opposite effect happened during diastole, with gas being redirected to the other parts of the lungs.

The origin of CO_f has been a matter of debate for some time, stimulated by contradictory results from different groups (11). Whereas early studies suggested an aspirating effect of the heart during systole, simply explained by a pressure change induced by a volume change of the lung, more recent works claim that CO_f are caused by pulmonary artery pulsatility (23, 29). It is doubtful that pulmonary artery pulsatility could explain our observations of regional phase difference between the left lower part and the rest of the lungs. Moreover the fact that these latter studies are based on pressure and flow measurements at the mouth only, and were performed during open chest conditions, raises the question as to whether the same, related or indeed potentially different phenomena are being observed and compared. An alternative and more satisfactory mechanism is given by Engel (11): the oscillatory motion of the heart, in addition to volume changes, produces deflation and inflation in the surrounding parts of the lung, resulting in a dynamic redistribution of the gas. It is clear from the segmentation of the cardiac gated proton images that the mechanical action of the heart produces a volume change mainly affecting the left lower part of the lungs (see Fig. 6 and online supplementary video); we believe that this results in pressure changes causing the observed redistribution of gas within the lung. During systole, the blood redistribution from the ventricles to the systemic and pulmonary circulation results in a stretch of the left lower part of the lung. Simultaneously, more gas is observed to flow into this part of the lung. During diastole, the heart volume increases at the expense of the surrounding left lobe where expiratory flows are measured.

It is interesting to compare the proposed mechanism with recent models of pendelluft in the bronchial tree (14). The pendelluft effect has been reported at different airway levels mainly in pulmonary diseases or under abnormal conditions and is expected to occur when regions of the lung have different dynamics of regional inflation and deflation (for example, regions with

different compliance and/or flow resistance due to lung disease). In this sense, the asymmetric volume change created by the cardiac cycle could lead to regional pressure differences and explain the pendelluft observed at the carina bifurcation, therefore reflecting the modelling predictions by Greenblatt et. al. (14). However, the main difference in the observed pendelluft in the present study is that it results from the natural cardiac motion in subjects with healthy lungs.

The resulting oscillatory gas flows constitute an additional mechanism for gas mixing in the lung (12, 13, 15) but quantitative measurements are required to conclude on their significance. A recent study supports that the heart-lung interactions are a vital source of gas mixing (26). In addition, aerosol transport, mixing and deposition could be strongly affected by CO_f, which is particularly relevant for inhaled therapeutics. Ma et al. (18) and Darquenne et al. (8) proposed the existence of cardiogenic mixing to explain differences between measurement and simulations of aerosol dispersion, and for the heterogeneity of particle deposition in microgravity, respectively. In a following study, Darquenne et al. (7) addressed the effect of CO_f on the deposition and dispersion of 1-μm particles during breath holds. Although gravitational sedimentation is inferred to be the main mechanism, data have suggested that CO_f has a larger effect in the central airways than in the periphery of the lung. We believe that the effect of CO_f has been largely underestimated in the literature, especially in the field of CFD simulations of airflow in the main airways (9, 17, 25), where the influence of the heart has not, to our knowledge, been taken into consideration. Finally, it would be interesting to study how the observed mechanism could contribute to the chaotic mixing of fine particles proposed by Tsuda et al. (27). The classical theory assumes that acinar flow is kinematically reversible due to low Reynolds number gas flow deep in the lung. However, Tsuda et al. (28) and Butler et al. (2) observed kinematic irreversibility and complex convective stretch and fold patterns in excised rat

lungs supporting the theory that chaotic alveolar flow arising from flow trajectory asynchrony governs aerosol transport and mixing in the lung periphery.

Further work to simulate the influence of CO_f on airflow patterns is required to supplement our findings, but we hope this study will increase awareness of the effect of cardiac motion on gas flow and distribution within the lungs among the pulmonary community.

Grants

This work was funded by EU FP7 AirPROM, EPSRC # EP/D070252/1 and by the National Institute of Health Research (NIHR). This article presents independent research funded by the NIHR. The views expressed are those of the authors and not necessarily those of the NHS, the NIHR or the Department of Health.

Disclosures

No conflicts of interest, financial or otherwise, are declared by the authors.

References

1. **Bijaoui E, Baconnier PF, and Bates JH**. Mechanical output impedance of the lung determined from cardiogenic oscillations. J Appl Physiol (1985) 91: 859-865, 2001.
2. **Butler JP, and Tsuda A**. Logistic trajectory maps and aerosol mixing due to asynchronous flow at airway bifurcations. Respir Physiol Neurobiol 148: 195-206, 2005.
3. **Collier GJ, and Wild JM**. In vivo measurement of gas flow in human airways with hyperpolarized gas MRI and compressed sensing. Magn Reson Med (July 1, 2014). doi: 10.1002/mrm.25348
4. **Corley RA, Kabilan S, Kuprat AP, Carson JP, Minard KR, Jacob RE, Timchalk C, Glenny R, Pipavath S, Cox T, Wallis CD, Larson RF, Fanucchi MV, Postlethwait EM, and Einstein DR**. Comparative Computational Modeling of Airflows and Vapor Dosimetry in the Respiratory Tracts of Rat, Monkey, and Human. Toxicol Sci 128: 500-516, 2012.
5. **Cotes JE, Chinn DJ, Miller MR, and Wiley InterScience (Online service)**. Lung function physiology, measurement and application in medicine. Malden, Mass. ; Oxford: Blackwell Pub., 2006.
6. **Dahlstrom H, Murphy JP, and Roos A**. Cardiogenic Oscillations in Composition of Expired Gas - the Pneumocardiogram. J Appl Physiol (1985) 7: 335-339, 1954.

7. **Darquenne C, Paiva M, and Prisk GK**. Effect of gravity on aerosol dispersion and deposition in the human lung after periods of breath holding. J Appl Physiol (1985) 89: 1787-1792, 2000.
8. **Darquenne C, West JB, and Prisk GK**. Deposition and dispersion of 1-micrometer aerosol boluses in the human lung: effect of micro- and hypergravity. J Appl Physiol (1985) 85: 1252-1259, 1998.
9. **De Backer JW, Vos WG, Vinchurkar SC, Claes R, Drollmann A, Wulfrank D, Parizel PM, Germonpre P, and De Backer W**. Validation of computational fluid dynamics in CT-based airway models with SPECT/CT. Radiology 257: 854-862, 2010.
10. **de Rochefort L, Maitre X, Fodil R, Vial L, Louis B, Isabey D, Croce C, Darrasse L, Apiou G, Caillibotte G, Bittoun J, and Durand E**. Phase-contrast velocimetry with hyperpolarized 3He for in vitro and in vivo characterization of airflow. Magn Reson Med 55: 1318-1325, 2006.
11. **Engel A**. Dynamic distribution of gas flow. In: Compr Physiol 2011, Supplement 12: Handbook of Physiology, The Respiratory System, Mechanics of Breathing: 575-593. First published in print 1986. doi: 10.1002/cphy.cp030332
12. **Engel LA, Menkes H, Wood LD, Utz G, Joubert J, and Macklem PT**. Gas mixing during breath holding studied by intrapulmonary gas sampling. J Appl Physiol (1985) 35: 9-17, 1973.
13. **Engel LA, Wood LD, Utz G, and Macklem PT**. Gas mixing during inspiration. J Appl Physiol (1985) 35: 18-24, 1973.
14. **Greenblatt EE, Butler JP, Venegas JG, and Winkler T**. Pendelluft in the bronchial tree. J Appl Physiol (1985) 2014.
15. **Kelly SM, Brancatisano AP, and Engel LA**. Effect of cardiogenic gas mixing on arterial O2 and CO2 tensions during breath holding. J Appl Physiol (1985) 62: 1453-1459, 1987.
16. **Koumellis P, van Beek EJR, Woodhouse N, Fichele S, Swift AJ, Paley MNJ, Hill C, Taylor CJ, and Wild JM**. Quantitative analysis of regional airways obstruction using dynamic hyperpolarized He-3 MRI - Preliminary results in children with cystic fibrosis. Journal of Magnetic Resonance Imaging 22: 420-426, 2005.
17. **Lambert AR, O'Shaughnessy P, Tawhai MH, Hoffman EA, and Lin CL**. Regional deposition of particles in an image-based airway model: large-eddy simulation and left-right lung ventilation asymmetry. Aerosol Sci Technol 45: 11-25, 2011.
18. **Ma BS, and Darquenne C**. Aerosol bolus dispersion in acinar airways-influence of gravity and airway asymmetry. J Appl Physiol (1985) 113: 442-450, 2012.
19. **Minard KR, Kuprat AP, Kabilan S, Jacob RE, Einstein DR, Carson JP, and Corley RA**. Phase-contrast MRI and CFD modeling of apparent (3)He gas flow in rat pulmonary airways. J Magn Reson 221: 129-138, 2012.
20. **Montmerle S, and Linnarsson D**. Effects of gravity and blood volume shifts on cardiogenic oscillations in respired gas. J Appl Physiol (1985) 99: 931-936, 2005.
21. **Mylavarapu G, Murugappan S, Mihaescu M, Kalra M, Khosla S, and Gutmark E**. Validation of computational fluid dynamics methodology used for human upper airway flow simulations. J Biomech 42: 1553-1559, 2009.
22. **Quanjer PH, Stanojevic S, Cole TJ, Baur X, Hall GL, Culver BH, Enright PL, Hankinson JL, Ip MS, Zheng J, and Stocks J**. Multi-ethnic reference values for spirometry for the 3-95-yr age range: the global lung function 2012 equations. The European respiratory journal 40: 1324-1343, 2012.
23. **Suarez-Sipmann F, Santos A, Peces-Barba G, Bohm SH, Gracia JL, Calderon P, and Tusman G**. Pulmonary artery pulsatility is the main cause of cardiogenic oscillations. J Clin Monit Comput 27: 47-53, 2013.
24. **Sun Y, Butler JP, Ferrigno M, Albert MS, and Loring SH**. "Ventilatory alternans": a left-right alternation of inspiratory airflow in humans. Respir Physiol Neurobiol 185: 468-471, 2013.
25. **Tawhai MH, and Lin CL**. Airway gas flow. Compr Physiol 1: 1135-1157, 2011.
26. **Thurgood J, Dubsky S, Henon Y, Jesudason E, and Fouras A**. Heart-lung interactions: A vital source of gas mixing within the lungs. Am J Respir Crit Care Med 189: A6275, 2014.
27. **Tsuda A, Laine-Pearson FE, and Hydon PE**. Why chaotic mixing of particles is inevitable in the deep lung. J Theor Biol 286: 57-66, 2011.

28. **Tsuda A, Rogers RA, Hydon PE, and Butler JP**. Chaotic mixing deep in the lung. P Natl Acad Sci USA 99: 10173-10178, 2002.
29. **Tusman G, Suarez-Sipmann F, Peces-Barba G, Climente C, Areta M, Arenas PG, and Bohm SH**. Pulmonary blood flow generates cardiogenic oscillations. Respir Physiol Neurobiol 167: 247-254, 2009.
30. **West JB, and Hugh-Jones P**. Pulsatile gas flow in bronchi caused by the heart beat. J Appl Physiol (1985) 16: 697-702, 1961.
31. **Wild JM, Paley MN, Kasuboski L, Swift A, Fichele S, Woodhouse N, Griffiths PD, and van Beek EJ**. Dynamic radial projection MRI of inhaled hyperpolarized 3He gas. Magn Reson Med 49: 991-997, 2003.

Figure Captions

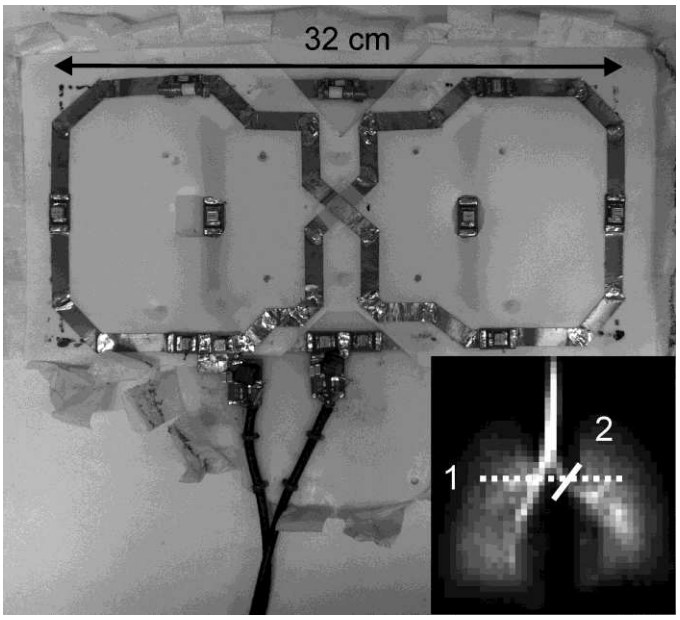

Figure 1:

Picture of the quadrature transmit/receive radiofrequency coil used for 2D flow measurement in the left main bronchus (see slice location 2, solid line in the inset). Inset: example of a HP ^{3}He ventilation image with indication of slice locations used for 1D (1) and 2D (2) phase contrast velocimetry sequences.

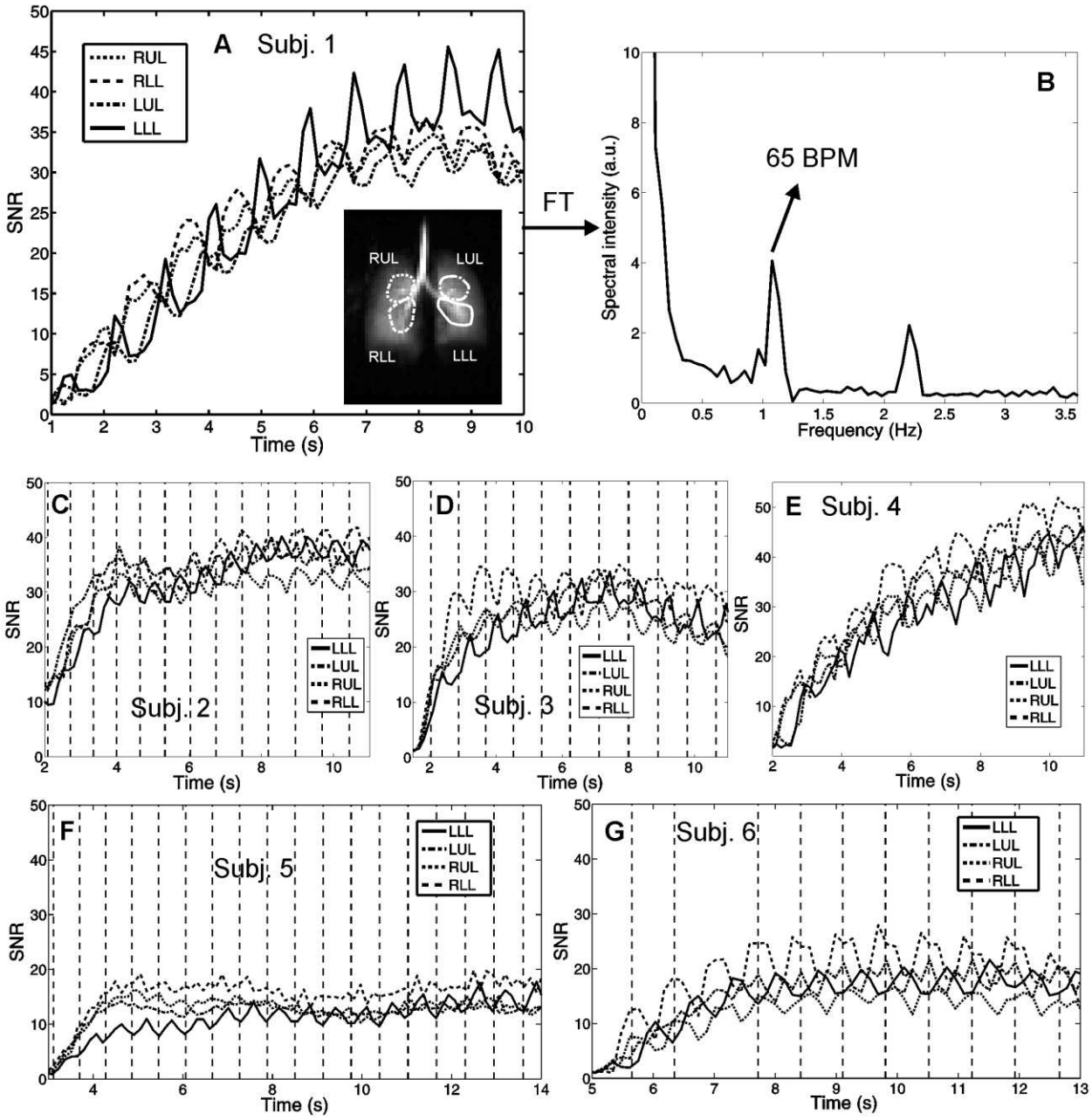

Figure 2:

A: Time evolution of the SNR in the 4 ROIs (RUL, LUL, RLL and LLL) of the Cartesian dynamic images of subject 1 (example image and ROI positions shown in the inset). **B**: Frequency spectrum of the signal corresponding to the left lower part of the lung (curve LLL in **A**) after a Fourier transform (FT). The peaks at 1.08 and 2.2 Hz correspond to the fundamental

and the second harmonic of the heart rate of the subject (65 BPM). **C** to **G**: Time evolution of the signal in the 4 ROIs for subjects 2 to 6. For subjects 2, 3, 5 and 6 the ECG was recorded and the dashed vertical lines correspond to the occurrence of R-waves. Note: an R-wave occurrence is missing (not recorded) in G (subject 6) at ~ 7 s.

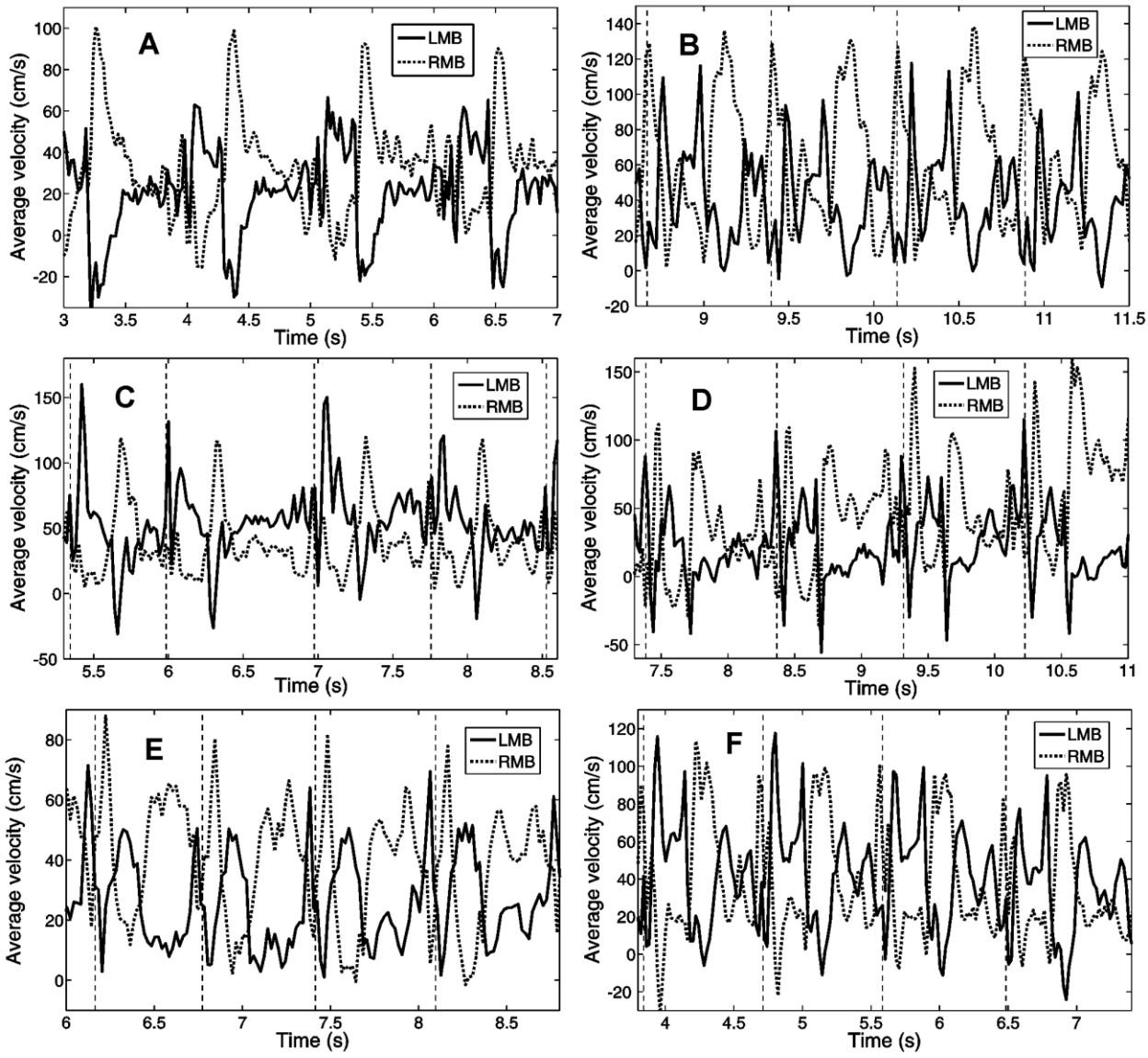

Figure 3:

1D PCV. Time evolution of the average velocity of ^{3}He gas in the left/right main bronchi (LMB/RMB) in subjects 1 to 6 (A to F respectively) during a constant inhalation (see slice location 1 in the inset of Fig. 1). The vertical dashed lines correspond to the occurrences of the R-waves that were recorded with ECG (not recorded for subject 1). For subject 3 (C) a case of arrhythmia can be observed between 6 to 7 s. Mean estimated errors for each average velocity curve were: A LMB: ± 5 cm s^{-1}; RMB: ± 5 cm s^{-1}. B LMB: ± 8 cm s^{-1}; RMB: ± 7 cm s^{-1}. C LMB: ± 6 cm s^{-1}; RMB: ± 5 cm s^{-1}. D LMB: ± 8 cm s^{-1}; RMB: ± 6 cm s^{-1}. E LMB: ± 7 cm s^{-1}; RMB: ± 6 cm s^{-1}. F LMB: ± 5 cm s^{-1}; RMB: ± 5 cm s^{-1}.

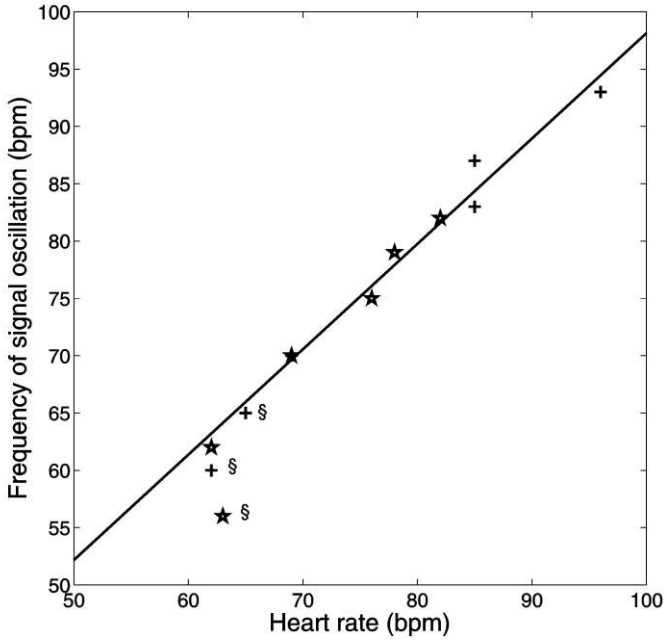

Figure 4:

Correlation and linear regression line of the fundamental frequency of the signal oscillations and the heart rate measured with ECG. Crosses: from the SNR oscillations of LLL during the dynamic ventilation experiments. Stars: from the 1D velocity measurement (in left main bronchus). Solid line: linear regression line (f(SNR) = 6.24 + 0.92 × HR, correlation coefficient:

0.99). §: Heart beat measured by finger probe shortly before the experiments and not by synchronized ECG recording. The three values marked with "§" are shown on the graph but were not included into the regression line, nor were they used in the calculation of the correlation coefficient.

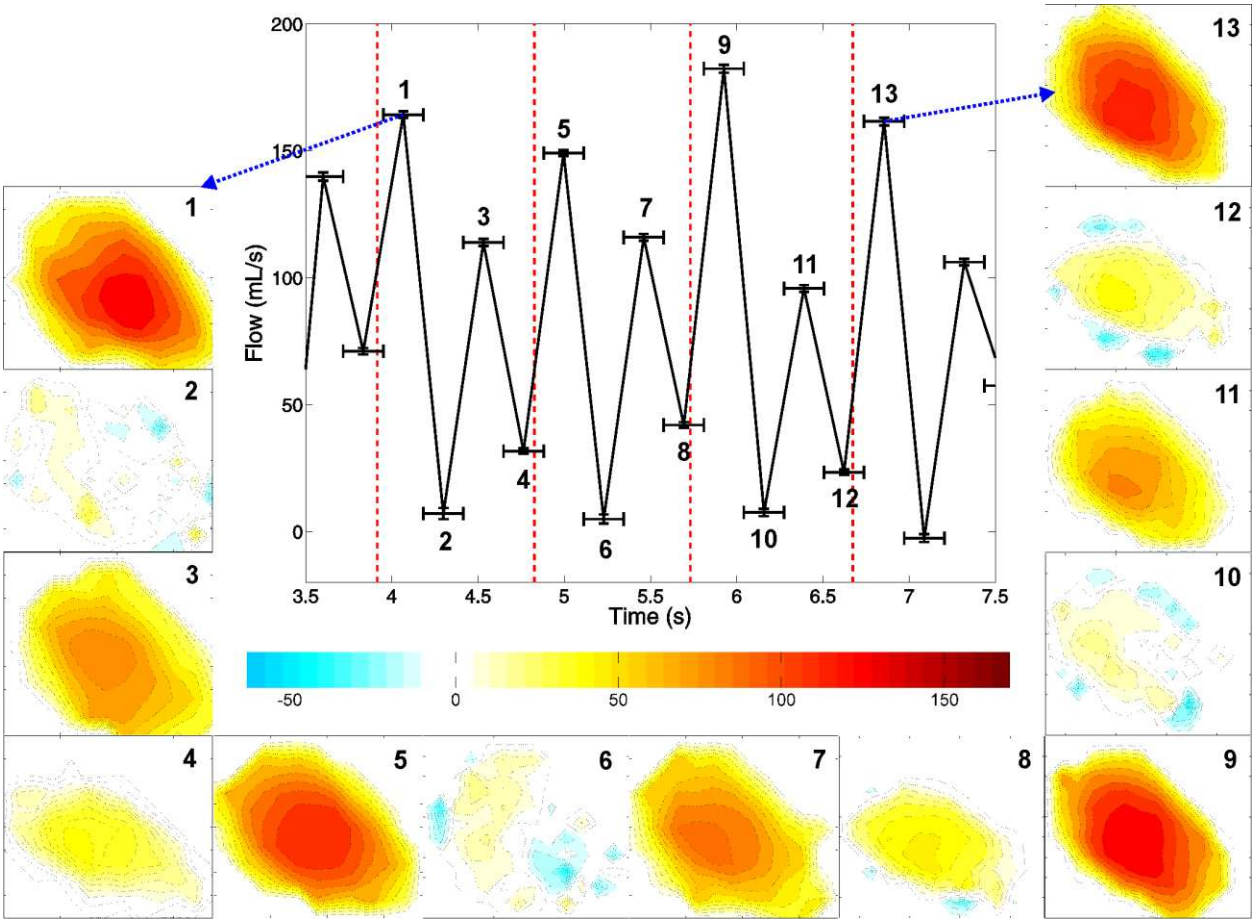

Figure 5:

2D PCV. Time evolution of the ^{3}He gas flow in the left main bronchus of subject 7 measured during a constant inhalation (see slice location 2 in the inset of Fig. 1, time resolution of 232.4 ms). Example velocity maps (1 - 13), from which the values of the flow curve were calculated, are shown around the plot (color bar in cm s^{-1}). The average uncertainty σ_v in velocity values for

the given velocity maps was ~ 5 cm s^{-1}. The flow error bars (on the vertical axis) were calculated according to the method described in the image analysis section and range between ± 1 and ± 2 mL s^{-1}. The "x-error bars" on the flow curve represent the acquisition window for each velocity map.

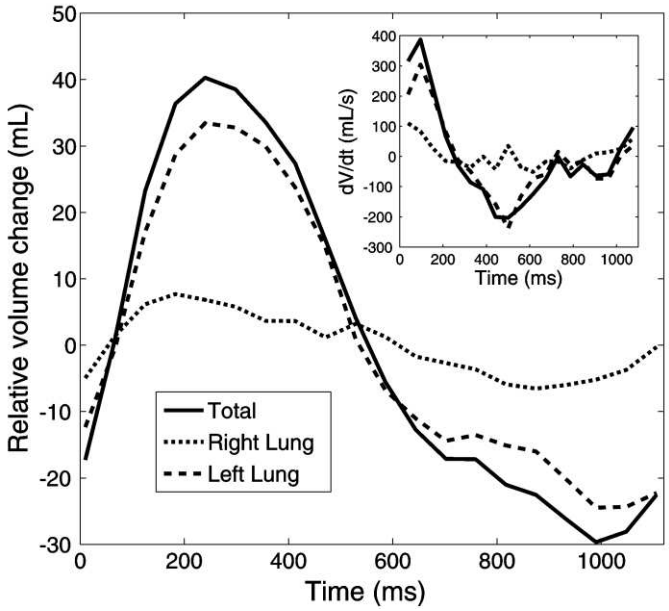

Figure 6:

Relative left and right lung volume changes and the corresponding time-derivatives (inset) after segmentation of a cardiac gated series of proton images of the lungs of subject 1 acquired during breath hold (20 cardiac phases).

Tables

Table 1:

Subject characteristics and sequences performed

M, male; F, female; FEV_1, forced expiratory volume in 1 s; FVC, forced vital capacity. * See ref. (22) . †

Synchronised ECG recording available.

Table 2:

Fourier transform analysis of the data from the dynamic ventilation experiments

* in beats per minute, † from finger probe shortly before the experiment, § from synchronized ECG recording. ‡ No clear oscillations were observed for subject 5 in the LUL, RLL and RUL explaining why no values are quoted.